Published in final edited form as:

Biochem J. ; 474(24): 4035–4051. doi:10.1042/BCJ20170426.

Direct visualization of interaction between calmodulin and connexin45

Juan Zou[1], **Mani Salarian**[1], **Yanyi Chen**[1], **You Zhuo**[1], **Nicole E. Brown**[2], **John R. Hepler**[2], and **Jenny J. Yang**[1]

[1]Department of Chemistry, Center for Diagnostics and Therapeutics, Georgia State University, Atlanta, GA 30303, USA

[2]Department of Pharmacology, Emory University School of Medicine, Atlanta, GA 30322, USA

Abstract

Calmodulin (CaM) is an intracellular Ca^{2+} transducer involved in numerous activities in a broad Ca^{2+} signaling network. Previous studies have suggested that the Ca^{2+}/CaM complex may participate in gap junction regulation via interaction with putative CaM-binding motifs in connexins; however, evidence of direct interactions between CaM and connexins has remained elusive to date due to challenges related to the study of membrane proteins. Here, we report the first direct interaction of CaM with Cx45 (connexin45) of γ-family in living cells under physiological conditions by monitoring bioluminescence resonance energy transfer. The interaction between CaM and Cx45 in cells is strongly dependent on intracellular Ca^{2+} concentration and can be blocked by the CaM inhibitor, *N*-(6-aminohexyl)-5-chloro-1-naphthalenesulfonamide hydrochloride (W7). We further reveal a CaM-binding site at the cytosolic loop (residues 164–186) of Cx45 using a peptide model. The strong binding (K_d ~ 5 nM) observed between CaM and Cx45 peptide, monitored by fluorescence-labeled CaM, is found to be Ca^{2+}-dependent. Furthermore, high-resolution nuclear magnetic resonance spectroscopy reveals that CaM and Cx45 peptide binding leads to global chemical shift changes of ^{15}N-labeled CaM, but does not alter the size of the structure. Observations involving both N- and C-domains of CaM to interact with the Cx45 peptide differ from the embraced interaction with Cx50 from another connexin family. Such interaction further increases Ca^{2+} sensitivity of CaM, especially at the N-terminal domain. Results of the present study suggest that both helicity and the interaction mode of the cytosolic loop are likely to contribute to CaM's modulation of connexins.

Correspondence: Jenny J. Yang jenny@gsu.edu.

Author Contribution

J.Z. conducted most of the experiments and analyzed the results. J.Z. and M.S. wrote the paper together. Y.C. contributed to the experiment design. Y.Z. conducted experiments on NMR and N.E.B. helped with designing and performing BRET experiments and analyzing BRET result. J.R.H. helped with BRET experiment design and manuscript editing. J.Y. supervised the research and wrote the manuscript.

Competing Interests

The Authors declare that there are no competing interests associated with the manuscript.

Introduction

Gap junctions formed by two hemichannels of connexins between two adjacent cells provide a direct pathway for cell communication and the cell-to-cell transfer of small molecules (<1 kDa). This specialized membrane structure integrates broad cellular functions, including cell differentiation, growth, and development, in nearly all mammalian tissue [1]. To date, ~21 human genes coding gap junction proteins have been discovered [2]. These share the same structural topology with four highly conserved transmembrane regions, a short N-terminal cytoplasmic region, one intracellular and two extracellular loops, and a C-terminal intracellular tail that exhibits the greatest sequence variation among the connexins. As a γ-family connexin, Cx45 (connexin45) has a much longer cytoplasmic loop region than α- and β-family connexin isoforms Cx43 and Cx50, and Cx26, respectively. The expression of Cx45 was first identified in chick embryos where its expression was found to be 10-fold lower in adults compared with early embryos [3]. Subsequently, Cx45 was identified as one of the main three connexin isoforms found in the heart, specifically in the sinoatrial node, the atrioventricular node, and His-bundle and bundle branches [4–8]. Studies have reported that Cx45-deficient mice typically died within 9–10 embryonic days due to heart abnormality, suggesting its important role in heart development [9–11]. Cx45 is also expressed in other tissues such as smooth muscle and brain [4,12,13].

Multiple factors, including intracellular Ca^{2+} concentrations ($[Ca^{2+}]_i$) and activation of CaM (calmodulin), have been reported to regulate intercellular communication mediated by gap junctions [14,15]. CaM is a key multifunctional transducer of Ca^{2+} signals in eukaryotes, responding to the changes in $[Ca^{2+}]_i$. An increase in $[Ca^{2+}]_i$ initiates the downstream signaling cascade [16–18]. Upon Ca^{2+} binding to its four EF-hand Ca^{2+}-binding motifs in two globular N- and C-domains, CaM undergoes a conformational change exposing hydrophobic patches that are essential to its ability to bind more than 300 target proteins in multiple cellular processes [19–21]. Because its N- or C-domains exhibit different Ca^{2+}-binding affinities and kinetic properties, CaM is able to differentiate between local and global Ca^{2+} changes to regulate various membrane channels/pumps with different interaction modes [20,22–26]. Results of a study by Kink et al., indicating that CaM can function as a modulator on Ca^{2+}-dependent Na^+ current or K^+ current [27], significantly expanded our perception of its potential role in the regulation of many other ion channels [28–33].

Various past studies have proposed that CaM may play an active role in the regulation of gap junctions comprised of all three connexin subfamilies [34–37]. Evidence of CaM's role in regulation of Cx45 was first reported by Peracchia et al. by monitoring the sensitivity of Cx45 channels to CO_2 and inhibiting CaM expression in oocytes [38]. Elevating $[Ca^{2+}]_i$ (within seconds) leads to a rapid inhibition of cell-to-cell communication with increased internal electrical resistance [39]. This process was prevented by pre-incubation with CaM antagonists [40–42]. Since then, several additional studies have reported that CaM participates in the operation of gap junctions [35,43–46]. We have also previously reported that gap junctions formed by α-family connexins such as Cx43, Cx44, or Cx50 can be effectively closed by elevating intracellular Ca^{2+} and CaM antagonist [47–49]. It remains hotly debated as to whether or not CaM directly interacts with connexins, which has been

difficult to measure due to the technical challenges and limitations of studying integral membrane proteins. Since connexins have four transmembrane segments, they often fail to assume a native conformation following expression and purification and have very limited solubility in solution. Moreover, the cytosolic intracellular loop and carboxyl terminus of connexins remain 'invisible' even in the recently determined X-ray structures of connexins [50,51]. Furthermore, CaM regulates numerous variable cellular target proteins, but there are currently few reagents available capable of inhibiting CaM with desired specificity. Consequently, the molecular mechanism of CaM-mediated regulation of Cx45 remains poorly understood.

In the present work, for the first time, we have demonstrated that there is direct interaction between Ca^{2+}/CaM and full-length Cx45 in HEK293 cells using BRET (bioluminescence resonance energy transfer) assay. We then identified the CaM-binding site using a peptide model and probed the molecular interactions between CaM and Cx45 using various spectroscopic methods, including high-resolution nuclear magnetic resonance (NMR). We further reported here the differential action of Ca^{2+}/CaM on the cytosolic loop of Cx45, which exhibits an extended conformation that is different from α-family connexins. Together, our findings provide important insights into the molecular mechanism of intracellular Ca^{2+} and CaM regulation of γ-family con-nexin—Cx45.

Materials and methods

Cell culture

HeLa cells from ATCG (Manassas, VA) were fed on Dulbecco's Modified Eagle Medium and 10% fetal bovine serum. The cells were cultured at 37°C in a humidified incubator with 5% CO_2.

Bioluminescence resonance energy transfer

The yellow fluorescent fusion protein expression vector Venus-C1 and the *Renilla* luciferase (Rluc) fusion protein expression vectors were used [52]. Construction of luciferase fusion protein vector mCx45-Rluc was achieved by insertion of the PCR product of the mouse Cx45 into vector Rluc-N1 at XhoI and HindIII enzyme sites upstream of luciferase. Venus–CaM (Venus to CaM) was generated by insertion of rat CaM gene into vector pVenus-N1 at NheI and XmaI. The BRET assay was carried out on a TriStar LB941 multimode microplate reader. The HEK293 cells cotransfected with Venus–CaM, and Cx45-Rluc were detached and suspended in sterilized BRET buffer (140 mM NaCl, 2.7 mM KCl, 1 mM $CaCl_2$, 1 mM $MgCl_2$, 0.37 mM NaH_2PO_4, 24 mM $NaHCO_3$, 25 mM HEPES, and 0.1% Glucose) and distributed into 96-well plates. Before measurement, coelenterazine was added to a final concentration of 5 μM and sequential measurements were performed at 460 ± 25 and 525 ± 25 nm. In some cases, cells were treated either with BAPTA-AM (50 μM) or $CaCl_2$ (5 mM $CaCl_2$ and 10 μM ionomycin) or W7 [*N*-(6-aminohexyl)-5-chloro-1-naphthalenesulfonamide hydrochloride] (50 μM) for 20, 10, and 30 min, respectively, before BRET measurement. The average BRET signals from three experiments were plotted as a function of the ratio of acceptor over the donor.

Prediction of CaM-binding motif

The Cx45 sequences were examined for CaM-binding sites based on common features by analysis of determined structure complexes and reported CaM-binding studies in addition to the CaM target database [53,54]. A sequence alignment was performed using Clustal W2 [55].

Cx45 peptide

The peptide derived from the cytoplasmic loop of Cx45 ($Cx45p_{164–186}$, Ac-^{164}GRRRIREDGLMKIYVLQLLARTV^{186}-NH_2) was obtained commercially from AnaSpec, Inc. The peptide was >90% pure on the basis of high-performance liquid chromatography and was used without further purification. Peptide size was verified by electrospray ionization mass spectrometry (ESI-MS). Acylated N-termini and aminated C-termini were designed to mimic the protein environment and remove extra charges.

Purified proteins

Unlabeled or ^{15}N isotopically labeled recombinant rat CaM and CaM half domains (N-CaM: resides from 1 to 75 and C-CaM: resides from 76 to 148) were expressed in *Escherichia coli* and were purified as described previously [47,56]. Protein concentrations were determined using the molar absorption coefficients ε_{277} of 3030 M^{-1} cm^{-1} for CaM.

Dansylated CaM (D-CaM) and CaM half domains (D-N-CaM and D-C-CaM) were synthesized according to the method described previously [57]. The dansylation of CaM was confirmed by ESI-MS. Concentrations of D-CaM, D-N-CaM, and D-C-CaM were measured by using the ε_{335} of 3980 M^{-1} cm^{-1}.

CD spectroscopy

CD spectra were recorded on a Jasco-810 spectropolarimeter at ambient temperature using a 0.1-cm path length quartz cuvette, an integration time of 1 s, and a scan rate of 100 nm/s. The far UV CD spectra of CaM (8 μM) and CaM–$Cx45p_{164–186}$ complex (8 μM) were obtained in 10 mM Tris, 100 mM KCl, at pH 7.5 with 5 mM $CaCl_2$ or 5 mM EGTA. The far UV CD spectra of the peptide in different percentages of TFE (trifluoroethanol) were obtained using a concentration of 20 μM $Cx45p_{164–186}$ in the same buffer. Multiple scans (10) were averaged and baselines were subtracted. Each spectrum shown is the ellipticity (mdeg) as a function of wavelength. The secondary structure contents of the peptide were calculated using DICHROWEB [58].

Fluorescence spectrometry

Steady-state fluorescence measurements were carried out in triplicate with a QM1 fluorescence spectrophotometer (PTI) at ambient temperature using a cell path length of 1 cm. Dansylated CaM samples (0.25 μM) were prepared in 10 mM Tris–HCl buffer (pH 7.5) containing 100 mM KCl, 5 mM Ca^{2+}, or 5 mM EGTA. Titration was carried out by gradually adding the peptide stock solution (25 μM) prepared in the same buffer. The excitation wavelength was 335 nm, with fluorescence emission intensity recorded between 400 and 600 nm. The binding constant of the synthetic peptide to modified CaM was

obtained with a 1 : 1 binding model by fitting normalized fluorescence data as described previously [47].

Equilibrium Ca^{2+} titrations were performed at room temperature using the same spectrophotometer as described above. CaM (8 μM) or with $Cx45p_{164–186}$ peptide (molar ratio of 1 : 1.2) in 50 mM HEPES (pH 7.4), 100 mM KCl, 5 mM nitrilotriacetic acid (NTA), and 0.05 mM EGTA were titrated with 15 or 50 mM calcium solution prepared in the same buffer. The intrinsic fluorescence of tyrosine (λ_{ex} = 277 nm, λ_{em}= 320 nm) or phenylalanine (λ_{ex} = 250 nm, λ_{em}= 280 nm) was used to monitor the Ca^{2+} binding to the CaM C- and N-domains, respectively [59]. The fluorescent Ca^{2+} indicator dye (0.2 μM) Oregon Green 488 BAPTA-5N (Oregon Green) was used to determine the free Ca^{2+} concentration at each titration point using eqn (1) as previously described.

$$\left[Ca^{2+}\right]_{free} = K_d \cdot \frac{F - F_{min}}{F_{max} - F} \quad (1)$$

In eqn (1), F represents the fluorescence intensity of Oregon Green at each titration point, while F_{max} and F_{min} represent the fluorescence intensity of dye at Ca^{2+}-saturated and Ca^{2+}-free states, respectively.

Ca^{2+} titrations of CaM samples were repeated at least three times and fitted to a non-linear Hill equation (eqn 2).

$$f = \frac{\left[Ca^{2+}\right]^n_{free}}{K_d + \left[Ca^{2+}\right]^n_{free}} \quad (2)$$

where f is the fractional change of intrinsic fluorescence intensity; $[Ca^{2+}]_{free}$ is the concentration of free ionized Ca^{2+} in solution; K_d represents the Ca^{2+} dissociation constants and n is the Hill coefficient.

Surface plasmon resonance

Using a Biacore T100 SPR (surface plasmon resonance) system, we determined the kinetics of CaM binding to $Cx45p_{164–186}$ which was immobilized on a CM5 sensor chip by amine coupling. Cx45 peptide was immobilized on a CM5 sensor chip to a final response unit of 2000. Various concentrations of CaM in HEPES buffer [10 mM HEPES, 150 mM KCl, and 5 mM $CaCl_2$ or EGTA (pH 7.5)] were injected for 10 min at 15 μl/min. The sensor chip was regenerated by 10-time injection of 30 mM NaOH for 30 s. All of the binding curves were collected by reference flow cell subtraction.

NMR spectroscopy

All ^{15}N-^{1}H HSQC spectra were recorded on either Varian Inova 600 or 800 MHz spectrometers. CaM NMR samples were prepared by diluting protein samples to 250 or 500 μM using buffer with the following composition: 10% D_2O, 5 mM MES, 10 mM Bis–Tris,

100 mM KCl, and 0.02% NaN_3 with 10 mM Ca^{2+} or 10 mM EGTA. The pH values were adjusted to 7.4. NMR spectra were acquired at 37°C. ^{15}N uniformly labeled CaM was titrated with different amounts of peptide derived from Cx45 in a series of peptide/CaM ratios (0, 0.5, 1, 1.5, and 2). NMR data were processed using NMRPipe [60] and analyzed using SPARKY [61] software package. Chemical shift perturbations (Δ) of the ^{1}H-^{15}N HSQC spectra with and without peptide were calculated using the same methods as described previously [49].

Mass spectrometry

The MALDI mass spectrometry analysis was performed on an Applied Biosystems 4800 plus MALDI TOF/TOF analyzer mass spectrometer (Framingham, MA). The data were acquired in a linear positive mode with sinapinic acid (SA) as a matrix for CaM (50 μM) and CaM–Cx45p complex. The molecular mass of the Cx45 peptide was also confirmed by MALDI with α-cyano-4-hydroxycinnamic acid (CHCA) as a matrix. CaM (50 μM) and Cx45 peptide (50 μM) were mixed in 100 mM KCl and 50 mM Tris–HCl, at pH 7.5. A 1 μl mixture was added with 10 μl of saturated SA solution and then dried on the MALDI plate for the measurements.

Statistical analysis

The data are presented as means ± SE of three independent experiments. Statistical analyses were carried out using the unpaired Student's *t*-test for comparison of two datasets. A *P*-value of <0.05 was considered statistically significant.

Results

Identification of a putative CaM-binding motif in the single cytoplasmic loop of Cx45

We identified a potential CaM-binding site within Cx45 based on several characteristics, including the hydropathy, α-helical propensity, residue weight, residue charge, hydrophobic, and helical residue contents [53]. Figure 1 reveals a conserved putative CaM-binding domain in the intercellular loop covering residues 164–186 of Cx45 (GRRRIREDGLMKIYVLQLLARTV). This putative CaM-binding motif possesses some of the characteristics of IQ-like motif ((F/I/L/V)Qxxx(R/K)Gxxxxxxx), but lacks conserved G after R/K [62–64]. On the other hand, it has some characteristics of motifs 1–10, 1–12, or 1–14 with hydrophobic residues spaced apart 10, 12, and 14 residues, respectively.

CaM interacts with Cx45 in live cells

To determine whether CaM associates directly with full-length Cx45 channels in live cells, we used the energy transfer-based technique BRET, in which the energy is transferred between bioluminescent and fluorescent tags in close proximity. We tagged the bioluminescent donor *Renilla reniformis* luciferase (Rluc) to Cx45 and the yellow fluorescent acceptor Venus–CaM (Figure 2A). HEK293 cells were cotransfected with a fixed amount of Cx45-Rluc and an increasing amount of Venus–CaM. As shown in Figure 2B, Venus–CaM is capable of producing a significant BRET signal determined as the ratio of light emitted at 525 nm over the light emitted at 460 nm. Elevating intracellular Ca^{2+} by preincubating cells with Ca^{2+}-ionomycin notably increased the BRET ratio 1-fold. In

contrast, decreasing intracellular Ca^{2+} (~0.27 nM) with 50 μM BAPTA-AM largely decreased BRET signal from 0.12 to ~0.03. The addition of CaM inhibitor (antagonist) W7 in the presence of Ca^{2+} also effectively reduces the BRET signal to the level of background noise (Figure 2B). We also verified the linear increases of the fluorescence intensity of the acceptor as a function of its expression. The same expression level of the donor Cx45-Rluc was confirmed by luminescence intensity. Taken together, these results indicated that CaM interacts with Cx45 in living cells and such interaction is Ca^{2+}-dependent and can be blocked by the specific CaM inhibitor W7.

Formation of 1 : 1 complex between CaM and Cx45p$_{164–186}$

To overcome the limitations associated with studying membrane protein interactions, we next probed the site-specific interaction of CaM to this putative binding motif of Cx45 using a peptide model. Peptide Cx45p$_{164–186}$ encompassing the predicted CaM-binding region was synthesized and characterized by various spectroscopic methods.

Interaction between CaM and Cx45p$_{164–186}$ and the associated stoichiometry was examined by mass spectrometry and NMR. Figure 3A (inset) shows that CaM and peptide Cx45p$_{164–186}$ forms a 1 : 1 complex in the presence of 5 mM Ca^{2+} with a molecular mass of 19.69 kDa, which is in a good agreement with the calculated mass of a 1 : 1 complex (19.69 kDa). In contrast, the observed complex was significantly smaller when incubated with EGTA.

High-resolution HSQC NMR with ^{15}N labeled CaM enables us to identify residue by residue interaction. A large number of dispersed resonances exhibited large chemical shift changes in the presence of Ca^{2+} following the addition of unlabeled peptide Cx45p$_{164–186}$. In contrast, there is no such significant changes were observed for resonances of CaM in the presence of 5 mM EGTA (Figure 3B). In the presence of Ca^{2+}, a progressive disappearance of the amide signal from residue A57 of CaM at 8.6 ppm was accompanied by the concomitant emergence of a new peak at 8.4 ppm upon the addition of peptide Cx45p$_{164–186}$ (Figure 3C). This slow chemical exchange behavior reached saturation at a ratio of 1 : 1 peptide:CaM complex. This further confirmed that the direct interaction between CaM and Cx45p$_{164–186}$ was Ca^{2+} dependent, and indicated a 1 : 1 stoichiometry. This slow exchange phenomenon is consistent with a strong protein–peptide interaction [48,65].

Measurements of CaM-binding affinity to Cx45 peptide

Fluorescence and Biacore studies were conducted to determine kinetic properties and binding affinity of CaM to Cx45p$_{164–186}$ peptide. Taking advantage of the dansyl emission near 500 nm that is very sensitive to the local conformational changes associated with formation of a protein–ligand complex, we labeled CaM with a dansyl moiety (D-CaM) [57,66]. The emission of D-CaM shifts from 520 to 500 nm as a consequence of Ca^{2+}-induced conformational change. The subsequent addition of Cx45p$_{164–186}$ further enhanced the intensity of D-CaM and shifted the emission peak to 496 nm (Figure 4A, inset), whereas the peptide did not induce any dansyl florescence change when Ca^{2+} was absent (Figure 4B). The fluorescence enhancement plotted against the concentration of D-CaM coincided with a 1 : 1 binding model, yielding a K_d of 5.0 ± 0.6 nM (Figure 4A). This strong

interaction is consistent with the slow chemical shift exchanges observed in the HSQC spectra (Figure 3C).

The interaction between CaM and the $Cx45p_{164–186}$ was further confirmed by SPR assay using Biacore 2000 sensor technology. The $Cx45p_{164–186}$ was immobilized to a CM5 sensor chip. The rapid and reversible association of CaM to $Cx45p_{164–186}$ was observed in the presence of 5 mM Ca^{2+} (Figure 5), but not in the presence of 5 mM EGTA. Rapid dissociation was also observed when using CaM-free buffer to wash the chip. No significant binding was observed between CaM and the chip surface.

Probing conformational change upon protein–ligand interaction

Secondary structure of the peptide conformation was evaluated in solution using far UV circular dichroism (CD) (Figure 6A). Deconvolution of the far UV CD spectrum suggested that $Cx45p_{164–186}$ is 45% α-helical, 5.2% β-strand, and ~50% unordered. Its conformation was not altered upon the addition of Ca^{2+}. Since TFE has proved to induce and stabilize the intrinsic helical conformation of peptides [67–70], we then examined the helical formation by far UV CD in the presence of increasing percentages of TFE. The addition of 20% TFE dramatically increases helical content from 45 to 75%, suggesting high helical propensity of Cx45 peptide (Figure 6A, inset).

Figure 6B shows that a 10.8% increase of α-helix signal was observed after the addition of $Cx45p_{164–186}$ to Ca^{2+}/CaM, while the addition of $Cx45p_{164–186}$ to apo-CaM resulted in a slight decrease of helicity. The helix increase of Ca^{2+}/CaM is likely due to the stabilization of helix formation or change of helix packing as observed in trigger proteins CaM [47,49] and TnC [71].

Interaction mode between $Cx45p_{164–186}$ and CaM

Detailed assignment of ^{15}N-labeled CaM NMR spectra in the presence and absence of peptide $Cx45p_{164–186}$ was achieved for ~54 residues using our established methods for Cx43 and Cx50 [47,49]. The weight-averaged chemical shift change was plotted as a function of residue number in Figure 7. The overall change of the N-lobe residues (4.68 ppm) was greater than that in the C-lobe residues (2.30 ppm). It is interesting to note that residues at the N- and C-domain as well as the linker region of CaM exhibited chemical shift changes greater than 0.05 ppm in the presence of $Cx45p_{164–186}$, suggesting a global conformation change upon formation of Ca^{2+}/CaM–$Cx45p_{164–186}$ complex. These broad changes of CaM induced by Cx45 binding are very different from the localized change of CaM induced by Cx43 and Cx50 binding with an embraced conformation similar to CaM kinase II [49]. In addition, Cx45 induces larger chemical shift changes of CaM than Cx50 [49].

We then determined the hydrodynamic radius of CaM and its changes upon formation of CaM–ligand complex using the pulsed-field gradient NMR. Figure 8 shows that the hydrodynamic radius of CaM (22.6 ± 0.6 Å) did not change significantly after formation of the CaM–$Cx45p_{164–186}$ complex. Conversely, Cx50 exhibited a significant decrease in hydrodynamic radius of 5.3 Å that is consistent with a collapsed complex formation [49]. This result further suggested that binding of $Cx45p_{164–186}$ to CaM involves an extended

conformation that is different from α-connexin Cx50 with an embraced compact form [34,49].

Effect of $Cx45p_{164–186}$ on the domain-specific Ca^{2+}-binding affinity of CaM

Ca^{2+}-binding affinities of both N- and C-domains of CaM upon formation of complex with $Cx45p_{164–186}$ were determined by monitoring the intrinsic fluorescence intensity change of Phe and Tyr, respectively. Binding of Ca^{2+} to the N-domain (Sites I and II) decreases Phe fluorescence intensity in the absence and presence of 1 : 1 molar ratio of $Cx45p_{164–186}$ (Figure 9A). On the other hand, binding Ca^{2+} to the C-domain (Sites III and IV) increases Tyr fluorescence intensity in the absence and presence of 1 : 1 molar ratio of $Cx45p_{164–186}$ (Figure 9B). Both Phe and Tyr fluorescence intensity changes of CaM as a function of free Ca^{2+} concentrations determined by Ca^{2+}indicator Oregon Green could be fit with a Hill equation. In the absence of $Cx45p_{164–186}$, CaM has a domain-specific affinity for Ca^{2+} of 11 and 2.3 μM. The formation of complex with $Cx45p_{164–186}$ results in 15-fold and 2-fold increases in Ca^{2+} affinity of N- and C-domains with K_d ~0.7 and 1.2 μM, respectively (Table 1).

Discussion

Regulation of connexins by Ca^{2+}/CaM and challenges in probing interactions

The role of CaM in the regulation of connexin channels was proposed 35 years ago by Peracchia et al. [72] based on the observation that CaM inhibitor trifluoperazine (TFP) protected amphibian embryonic cells from electrical uncoupling. They subsequently applied additional CaM blockers, calmidazolium, and W7 to prevent uncoupling of *Xenopus* embryonic cells [73] and crayfish axons [74,75], suggesting the generalized nature of CaM's role in regulating gap junctions. The gap junction protein Cx32 bound to CaM was later observed in gel overlays [76–78]. The suppression of CaM expression in oocytes can also inhibit CO_2-induced electrical uncoupling, which can subsequently be recovered by injection of CaM [44]. The effect of inhibiting CaM expression on CO_2-induced electrical uncoupling of *Xenopus* oocyte pairs expressing Cx45 demonstrated that both chemical and V_j sensitivities of Cx45 channels are reduced predominantly by inhibition of CaM expression through injecting of oligonucleotides that are antisense to CaM mRNAs [38]. The versatile binding capability of CaM to bind numerous targets, and the associated potential for perturbing other multiple targeting processes by CaM inhibitors, has suggested the potential for indirect rather than direct interaction with connexins. For example, both CaM- and CaM-dependent kinase II were reported to interact with Cx36 in an overlapping sequence region [79,80]. Unfortunately, the cytosolic regions for potential regulation locations in several determined structures of connexins are 'invisible' likely due to conformational ensembles [50,51]. The analyses of CaM interactions with connexins and associated Ca^{2+} dependence of this regulation in cells require a sensitive method of detection, and detailed examination of CaM's sensitivity to Ca^{2+} in the presence and absence of connexins.

Direct visualization of Ca^{2+}-dependent interaction of CaM with Cx45 in cells

In the present study, we report for the first time the direct interaction of CaM with Cx45 expressed in live cells under physiological conditions using a BRET-based assay. The BRET method uses non-radioactive (dipole– dipole) transfer of energy from a donor Luciferase enzyme to a suitable acceptor molecule such as YFP (Venus) after oxidation of the substrate. In BRET, resonance energy transfer efficiency depends on several factors based on the Förster rate equation, such as donor lifetime, distance between donor and acceptor, relative orientation, and degree of spectral overlap [81]. This technique overcomes problems such as photobleaching, auto-fluorescence, and especially simultaneous excitation of both donor and acceptor fluorophores [81]. This technique has been applied to study many protein–protein interactions in various cellular compartments of live cells, from G protein-coupled receptors [82–84] to nuclear cofactors [85]. While our findings here using BRET cannot completely rule out the possible contribution of a third protein mediating CaM and Cx45 interactions in live cells, the strong BRET signal we observed can only occur when proteins are within less than 10 nm, which is consistent with direct binding. Our complementary studies with peptide further reinforce that the CaM–Cx45 interaction is direct.

We have observed that the interaction between CaM and Cx45 can be monitored by tagging YFP (Venus) at either end of CaM (data not shown). The resulting BRET ratio is strongly CaM-dependent because it can be completely eliminated by the addition of CaM inhibitor W7. Such interaction is also strongly Ca^{2+}-dependent, because it can also be completely eliminated by reduction of intracellular Ca^{2+} using BAPTA. It is interesting to note that the detected maximum BRET ratio for CaM–Cx45 complex in HEK293 cells is about half of the maximum value in the presence of excess Ca^{2+} with ionomycin. This strong Ca^{2+}-dependent result suggests that CaM is well positioned in a sensitive state from which it can regulate Cx45 following changes in cellular conditions.

Increased Ca^{2+}sensitivity of CaM upon formation of CaM/Cx45$p_{164–186}$ complex

The Ca^{2+}-affinities of the two terminal domains of CaM can have differential sensitivities to the microenvironment of various target proteins [26,86–89]. By monitoring Phe and Tyr fluorescence signal changes, we determined N- and C-domain Ca^{2+}-binding affinities of CaM with K_d values of 11 and 2.8 μM, respectively. The addition of Cx45$p_{164–186}$ peptide to CaM increased the Ca^{2+}-binding affinity of both domains of CaM. However, the N-domain of CaM experienced a much greater decrease in dissociation constant (~15-fold) than the C-domain of CaM (~2-fold). This result is consistent with data from HSQC NMR (Figure 7), where the overall chemical shift changes in the N-lobe residues were greater than those of C-lobe residues. These results suggest a greater conformational change of the N-terminal lobe than that of C-lobe of CaM upon binding to Cx45$p_{164–186}$. We have also observed strong Ca^{2+}-dependent BRET signals using CaM tagged Venus (Figure 2). Additionally, results from the bell-based BRET assay along with the Ca^{2+}-binding affinity and NMR studies, when taken together, suggest that CaM's Ca^{2+} sensitivity, especially for the N-domain, is likely enhanced upon formation of a complex with Cx45. Thus, the overall cooperativity of both domains of CaM by Ca^{2+} is signifi-cantly enhanced. These findings are consistent with previous studies on CaM regulation with α-family connexins Cx43, 44, and 50 from α-subfamily [47–49], and other proteins, including Ca (V) 1.2 channels and RyR

[88–93]. Our results are very different from those reported for other proteins. For example, a reduction in Ca^{2+}-binding affinity of CaM was observed following complex formation with neuronal voltage-dependent sodium channels [64,94], which was achieved by lowering the Ca^{2+} affinity of the C-domain of CaM. Also, while it has been suggested that CaM may interact with Cx36, the physiological role of CaM binding is unclear since CaM kinase also directly interacts at the same region of the protein. Thus, it remains to be determined whether Ca^{2+} sensitivity of CaM is changed upon formation of a complex in the regulation of Cx36 [79,80].

CaM uses a novel extended action mode to regulate Cx45 that is different from the reported compact form of connexin

Structural characterization of CaM by NMR illustrated that, in the Ca^{2+}-bound state (holo-CaM), CaM exists in a dynamic equilibrium of two major conformations, an extended form and a semi-compact form, which provide sufficient flexibility for CaM to bind targets in variably extended conformations and to form interdomain connections [46]. Various target recognition modes have been attributed to CaM which can be classified into two general binding styles: extended and collapsed [95].

The novel CaM-binding motif from residues 164 to 186 in Cx45 has several characteristics of CaM-binding motifs. It is similar to the reported IQ-like motif pattern ((F/I/L/V)Qxxx(R/K)Gxxxxxxx) based on the absence of a conserved G residue following the charged R/K in the sequence. This identified CaM-binding site in Cx45 can also be classified as motifs 1–10, 1–12, and 1–14, because it has some characteristics of motifs 1–10, 1–12, or 1–14 with hydrophobic residues spaced apart 10, 12, and 14 residues, respectively. To the best of our knowledge, no such Ca^{2+}-dependent CaM-binding motif has been reported previously, especially for gap junction regulation. The conventional complete IQ motifs primarily associate with CaM primarily in a Ca^{2+}-independent manner, as seen with myosin. An important characteristic of the IQ motif is that it binds relatively tightly to CaM at basal levels of intracellular Ca^{2+}, and the interaction changes when Ca^{2+} levels are increased [95,96]. However, in some instances, IQ motif-containing proteins (including utrophim, Ras GRF1, Nina C myosins, and other proteins) have been reported to bind CaM in a Ca^{2+}-dependent manner. In those proteins, CaM can maintain its interaction with the IQ domains both in the presence and absence of Ca^{2+}, with dissociation constants ranging from sub-nanomolar to micromolar levels. However, the IQ motif-binding affinity of CaM varies with the Ca^{2+} concentration and the particular IQ motif in the target protein [36]. Additionally, Ca^{2+}-free CaM interacts with IQ motifs only through the C-domain [97], while Ca^{2+}-loaded CaM utilizes both N- and C-domains [98]. The IQ motif identified in the Cx45 cytosolic loop is incomplete, containing only the first part of an IQ motif (IQXXXR). When bound with a complete IQ motif, the C-domain of CaM is estimated to be in a semi-open conformation, while the N-terminal lobe is in a closed conformation. In contrast, it has been suggested that the N-domain of CaM would adopt an open conformation when only the first part of the IQ motif is present [99]. The $Cx45p_{164–186}$-binding affinity to CaM is also comparable to other IQ motifs found in channel proteins. For example, the disassociation constant of neuronal voltage-dependent sodium channel type II IQ motif for interaction with CaM is reported to be less than 10 nM.

The CaM-binding motif of Cx45 reported in the present paper exhibits a different mode of action than in previously reported gap junction studies. Our previous pulsed-field gradient NMR results indicated that the dynamic radius of holo-CaM decreased significantly upon Cx50-derived peptide binding [49]. For α-family connexins, the CaM-binding sites in Cx43, Cx44, and Cx50 follow a 1-5-10 binding motif in a compact form. CaM is also reported to have a compact form upon formation of a complex with a peptide encompassing the C-terminal region of Cx36 [79,80]. Conversely, results of our pulsed-field diffusion NMR studies suggested that the addition of the Cx45-derived peptide to Ca^{2+}–CaM did not change the dynamic radius of CaM which is consistent with an extended mode observed in other proteins such as the IQ motif of myosin V Ca^{2+} channels, anthrax toxin, SK channels (small conductance Ca^{2+}-activated potassium channels), Ca^{2+} pump, and glutamate decarboxylase [34]. CaM also exhibited widespread chemical shift changes upon binding with Cx45 peptide, which were significantly different from the domain localized changes observed with complex formation between CaM and Cx50, 43, and 44. The observed strong affinity of CaM binding for Cx45 is consistent with a greater degree of interactions and chemical shift changes.

Key factors in CaM contributing to interaction with $Cx45p_{164–186}$

Using fluorescence spectroscopy, we have demonstrated that $Cx45p_{164–186}$ binds to CaM with a K_d value of 5.0 ± 0.6 nM in the presence of Ca^{2+}. Compared with dissociation constants of different connexins from the same family (γ-family) that have been previously reported [45], $Cx45p_{164–186}$, which covers the intercellular loop, has stronger binding affinity for CaM than high-affinity sites of C-terminal domains in Cx34.7 (K_d = 29 ± 2 nM), Cx35 (K_d = 72 ± 9 nM), and Cx36 (K_d = 11 ± 3 nM) in the presence of Ca^{2+}. Comparison between $Cx45p_{164–186}$ and connexins from the α-family also suggests that the binding affinity of this peptide is stronger than $Cx43p_{136–158}$ (860 ± 20 nM) and $Cx44p_{132–153}$ (49 ± 3.0 nM) and similar to $Cx50p_{141–166}$ (4.9 ± 0.6 nM), which is also observed in the presence of Ca^{2+} [2]. In addition, $Cx45p_{164–186}$ binds much stronger to CaM than the N-terminal domain (K_d = 27 nM) and C-terminal region (K_d = 1200 nM) of Cx32 from the β-family [45].

The stronger binding affinity of $Cx45p_{164–186}$, compared with other connexins, may originate at least in part from the relative helical content of the peptide in solution without formation of complex with CaMas shown by CD spectroscopy (Figure 6A, inset) [34]. This strong helical content is much greater than connexins from α-family Cx50, Cx44, and Cx43. On the other hand, Cx50, Cx44, and Cx43 exhibit 94, 55, and 33% helical conformation, respectively, in the presence of 30% TFE [49]. Cx45 also has demonstrated to have the highest α-helical content induced by TFE and is similar to Cx50, indicating that the intrinsic helicity of the peptide may also contribute to the strong binding affinity of Cx45. This observation is consistent with previous reports that CaM binds to various target proteins whose binding domains have a strong propensity for forming α-helices [100]. CaM can also bind with high affinity to a relatively small α-helical region of many target proteins [36].

Implication for CaM regulation of connexins

Previous studies regarding the role of CaM in the regulation of Cx45 have been arguably inconclusive. Perrica and co-workers first reported the potential regulation of γ-connexin Cx45, by CaM, by monitoring the sensitivity of Cx45 channels to CO_2. Additionally, they reported that inhibiting CaM expression in oocytes using CaM inhibitor TFP, calmidazolium, or W7 reversibly inhibited the CO_2-induced electrical uncoupling in amphibian embryo cells by interfering with the mechanism which closes the cell-to-cell channels. Bader et al. also observed the regulation of the Cx45 hemichannel expressed in HeLa cells by intracellular Ca^{2+} [101]. However, their study excluded the role of CaM in regulation based on the rapid kinetics of co-regulation by extracellular Ca^{2+}. Therefore, results of our current study using in-cell BRET provide the first evidence that CaM is directly involved in the regulation of Cx45 in cells.

Based on our current results and previously published studies involving functional regulation, it is hypothe-sized that elevated $[Ca^{2+}]_i$ is initially sensed by CaM, and this promotes interaction between CaM and the CL domain of Cx45 to inhibit gap junction-mediated intercellular communication. Ca^{2+}/CaM binding to the $Cx45p_{164–186}$ region induces a gating response that closes the Cx45 gap junctions and follows the closure gating mechanism [34]. Further detailed studies are required to determine whether Ca^{2+}/CaM together with the CL domain of Cx45 function as a ‘cork’ to block the gap junction channel or if it induces a conformational change in the CL domain to occlude the cytoplasmic vestibule of Cx45 gap junction channel. Nevertheless, our study provides insights for defining the critical cellular changes and molecular mechanisms contributing to gap junctions. This information may greatly facilitate the development of new therapies to better manage and/or prevent human genetic diseases. In addition, the importance of Cx45 can be perceived by its presence in crucial locations of the human body such as the atrium in the working myocardium and in the conduction and central nervous system. Moreover, understanding the direct Ca^{2+}-dependent interaction of Cx45 with CaM may provide additional insights into the functional mechanism of Cx45 in brain and heart, and possibly an explanation as to how Cx45 in the cortex and hippocampus can contribute to the recovery of function following cell injury or neurological disorders associated with it [102].

Acknowledgments

We thank Dr Richard Veenstra (SUNY Upstate Medical University) for sharing the mouse Cx45 plasmid with us.

We thank Dr Camillo Peracchia for his helpful suggestions and Dr Michael Kirberger for editing.

Funding

This work was supported, in part, by NIH grants [EY-05684] to Charles F. Louis (C.F.L.) and Jenny J. Yang (J.J.Y.), [HL-042220] to Richard D. Veenstra (R.D.V.) and Jenny J. Yang, and [GM-081749] to Jenny J. Yang. This work was also supported by a Brain and Behavior Fellowship (GSU) to J. Zou, and a Molecular Basis of Disease Fellowship (GSU) to M. Salarian.

Abbreviations

$[Ca^{2+}]_i$	intracellular Ca^{2+} concentrations

BRET	bioluminescence resonance energy transfer
CaM	calmodulin
CD	circular dichroism
Cx45	connexin45
D-CaM	dansylated CaM
ESI-MS	electrospray ionization mass spectrometry
NMR	nuclear magnetic resonance
SA	sinapinic acid
SAN	sinoatrial node
SPR	surface plasmon resonance
TFE	trifluoroethanol
TFP	trifluoperazine
Venus–CaM	Venus to CaM
W7	*N*-(6-aminohexyl)-5-chloro-1-naphthalenesulfonamide hydrochloride

References

1. Neyton J, Trautmann A. Physiological modulation of gap junction permeability. J Exp Biol. 1986; 124:993–114. [PubMed: 2428910]
2. Sohl G, Willecke K. Gap junctions and the connexin protein family. Cardiovasc Res. 2004; 62:228–232. https://doi.org/10.1016/j.cardiores.2003.11.013. [PubMed: 15094343]
3. Beyer EC. Molecular cloning and developmental expression of two chick embryo gap junction proteins. J Biol Chem. 1990; 265:14439–14443. [PubMed: 2167316]
4. Coppen SR, Kodama I, Boyett MR, Dobrzynski H, Takagishi Y, Honjo H, et al. Connexin45, a major connexin of the rabbit sinoatrial node, is co-expressed with connexin43 in a restricted zone at the nodal-crista terminalis border. J Histochem Cytochem. 1999; 47:907–918. https://doi.org/10.1177/002215549904700708. [PubMed: 10375379]
5. van Veen TAB, van Rijen HVM, van Kempen MJA, Miquerol L, Opthof T, Gros D, et al. Discontinuous conduction in mouse bundle branches is caused by bundle-branch architecture. Circulation. 2005; 112:2235–2244. https://doi.org/10.1161/CIRCULATIONAHA.105.547893. [PubMed: 16203908]
6. Verheijck EE, van Kempen MJA, Veereschild M, Lurvink J, Jongsma HJ, Bouman LN. Electrophysiological features of the mouse sinoatrial node in relation to connexin distribution. Cardiovasc Res. 2001; 52:40–50. https://doi.org/10.1016/S0008-6363(01)00364-9. [PubMed: 11557232]
7. Honjo H, Boyett MR, Coppen SR, Takagishi Y, Opthof T, Severs NJ, et al. Heterogeneous expression of connexins in rabbit sinoatrial node cells: correlation between connexinisotype and cell size. Cardiovasc Res. 2002; 53:89–96. https://doi.org/10.1016/S0008-6363(01)00421-7. [PubMed: 11744016]
8. Coppen SR, Dupont E, Rothery S, Severs NJ. Connexin45 expression is preferentially associated with the ventricular conduction system in mouse and rat heart. Circ Res. 1998; 82:232–243. https://doi.org/10.1161/01.RES.82.2.232. [PubMed: 9468194]

9. Krüger O, Plum A, Kim JS, Winterhager E, Maxeiner S, Hallas G, et al. Defective vascular development in connexin 45-deficient mice. Development. 2000; 127:4179–4193. [PubMed: 10976050]
10. Kumai M, Nishii K, Nakamura K, Takeda N, Suzuki M, Shibata Y. Loss of connexin45 causes a cushion defect in early cardiogenesis. Development. 2000; 127:3501–3512. [PubMed: 10903175]
11. Nishii K, Kumai M, Egashira K, Miwa T, Hashizume K, Miyano Y, et al. Mice lacking connexin45 conditionally in cardiac myocytes display embryonic lethality similar to that of germline knockout mice without endocardial cushion defect. Cell Commun Adhes. 2003; 10:365–369. https://doi.org/10.1080/cac.10.4-6.365.369. [PubMed: 14681043]
12. Maxeiner S, Krüger O, Schilling K, Traub O, Urschel S, Willecke K. Spatiotemporal transcription of connexin45 during brain development results in neuronal expression in adult mice. Neuroscience. 2003; 119:689–700. https://doi.org/10.1016/S0306-4522(03)00077-0. [PubMed: 12809690]
13. Willecke K, Eiberger J, Degen J, Eckardt D, Romualdi A, Güldenagel M, et al. Structural and functional diversity of connexin genes in the mouse and human genome. Biol Chem. 2002; 383:725–737. https://doi.org/10.1515/BC.2002.076. [PubMed: 12108537]
14. del Corsso C, Iglesias R, Zoidl G, Dermietzel R, Spray DC. Calmodulin dependent protein kinase increases conductance at gap junctions formed by the neuronal gap junction protein connexin36. Brain Res. 2012; 1487:69–77. https://doi.org/10.1016/j.brainres.2012.06.058. [PubMed: 22796294]
15. Bennett MVL, Barrio LC, Bargiello TA, Spray DC, Hertzberg E, Sáez JC. Gap junctions: new tools, new answers, new questions. Neuron. 1991; 6:305–320. https://doi.org/10.1016/0896-6273(91)90241-Q. [PubMed: 1848077]
16. Klevit RE, Dalgarno DC, Levine BA, Williams RJP. ^{1}H-NMR studies of calmodulin. The nature of the Ca^{2+}-dependent conformational change. Eur J Biochem. 1984; 139:109–114. https://doi.org/10.1111/j.1432-1033.1984.tb07983.x. [PubMed: 6697998]
17. Wang CLA. A note on Ca^{2+} binding to calmodulin. Biochem Biophys Res Commun. 1985; 130:426–430. https://doi.org/10.1016/0006-291X(85)90434-6. [PubMed: 4026838]
18. Johnson CK. Calmodulin, conformational states, and calcium signaling. A single-molecule perspective. Biochemistry. 2006; 45:14233–14246. https://doi.org/10.1021/bi061058ehttp://dx.doi.org/. [PubMed: 17128963]
19. Bhattacharya S, Bunick CG, Chazin WJ. Target selectivity in EF-hand calcium binding proteins. Biochim Biophys Acta, Mol Cell Res. 2004; 1742:69–79. https://doi.org/10.1016/j.bbamcr.2004.09.002.
20. Ikura M, Ames JB. Genetic polymorphism and protein conformational plasticity in the calmodulin superfamily: two ways to promote multifunctionality. Proc Natl Acad Sci USA. 2006; 103:1159–1164. https://doi.org/10.1073/pnas.0508640103. [PubMed: 16432210]
21. Kawasaki H, Kretsinger RH. Calcium-binding proteins 1: EF-hands. Protein Profile. 1995; 2:297–490. [PubMed: 7553064]
22. Zuhlke RD, Reuter H. Ca^{2+}-sensitive inactivation of L-type Ca^{2+} channels depends on multiple cytoplasmic amino acid sequences of the α1C subunit. Proc Natl Acad Sci USA. 1998; 95:3287–3294. https://doi.org/10.1073/pnas.95.6.3287. [PubMed: 9501255]
23. Schonherr R, Lober K, Heinemann SH. Inhibition of human ether a go-go potassium channels by Ca^{2+}/calmodulin. EMBO J. 2000; 19:3263–3271. https://doi.org/10.1093/emboj/19.13.3263. [PubMed: 10880439]
24. Dai S, Hall DD, Hell JW. Supramolecular assemblies and localized regulation of voltage-gated ion channels. Physiol Rev. 2009; 89:411–452. https://doi.org/10.1152/physrev.00029.2007. [PubMed: 19342611]
25. Bers DM, Grandi E. Calcium/calmodulin-dependent kinase II regulation of cardiac ion channels. J Cardiovasc Pharmacol. 2009; 54:180–187. https://doi.org/10.1097/FJC.0b013e3181a25078. [PubMed: 19333131]
26. Tadross MR, Dick IE, Yue DT. Mechanism of local and global Ca^{2+} sensing by calmodulin in complex with a Ca^{2+} channel. Cell. 2008; 133:1228–1240. https://doi.org/10.1016/j.cell.2008.05.025. [PubMed: 18585356]

27. Kink JA, Maley ME, Preston RR, Ling KY, Wallen-Friedman MA, Saimi Y, et al. Mutations in paramecium calmodulin indicate functional differences between the C-terminal and N-terminal lobes *in vivo*. Cell. 1990; 62:165–174. https://doi.org/10.1016/0092-8674(90)90250-I. [PubMed: 2163766]
28. Budde T, Meuth S, Pape HC. Calcium-dependent inactivation of neuronal calcium channels. Nat Rev Neurosci. 2002; 3:873–883. https://doi.org/10.1038/nrn959. [PubMed: 12415295]
29. Saimi Y, Kung C. Calmodulin as an ion channel subunit. Annu Rev Physiol. 2002; 64:289–311. https://doi.org/10.1146/annurev.physiol.64.100301.111649. [PubMed: 11826271]
30. Wei F, Xia XM, Tang J, Ao H, Ko S, Liauw J, et al. Calmodulin regulates synaptic plasticity in the anterior cingulate cortex and behavioral responses: a microelectroporation study in adult rodents. J Neurosci. 2003; 23:8402–8409. [PubMed: 12968002]
31. Halling DB, Aracena-Parks P, Hamilton SL. Regulation of voltage-gated Ca^{2+} channels by calmodulin. Sci STKE. 2006; 2006:er15.
32. Tan BZ, Jiang F, Tan MY, Yu D, Huang H, Shen Y, et al. Functional characterization of alternative splicing in the C terminus of L-type $Ca_V1.3$ channels. J Biol Chem. 2011; 286:42725–42735. https://doi.org/10.1074/jbc.M111.265207. [PubMed: 21998309]
33. Ben-Johny M, Yue DT. Calmodulin regulation (calmodulation) of voltage-gated calcium channels. J Gen Physiol. 2014; 143:679–692. https://doi.org/10.1085/jgp.201311153. [PubMed: 24863929]
34. Zou J, Salarian M, Chen Y, Veenstra R, Louis CF, Yang JJ. Gap junction regulation by calmodulin. FEBS Lett. 2014; 588:1430–1438. https://doi.org/10.1016/j.febslet.2014.01.003. [PubMed: 24440348]
35. Peracchia C. Chemical gating of gap junction channels; roles of calcium, pH and calmodulin. Biochim Biophys Acta, Biomembr. 2004; 1662:61–80. https://doi.org/10.1016/j.bbamem.2003.10.020.
36. Rhoads AR, Friedberg F. Sequence motifs for calmodulin recognition. FASEB J. 1997; 11:331–340. [PubMed: 9141499]
37. Zimmer M, Hofmann F. Differentiation of the drug-binding sites of calmodulin. Eur J Biochem. 1987; 164:411–420. https://doi.org/10.1111/j.1432-1033.1987.tb11073.x. [PubMed: 3032617]
38. Peracchia C, Young KC, Wang XG, Peracchia LL. Is the voltage gate of connexins CO_2-sensitive? Cx45 channels and inhibition of calmodulin expression. J Membr Biol. 2003; 195:53–62. https://doi.org/10.1007/s00232-003-2044-6. [PubMed: 14502426]
39. Gandolfi SA, Duncan G, Tomlinson J, Maraini G. Mammalian lens inter-fiber resistance is modulated by calcium and calmodulin. Curr Eye Res. 1990; 9:533–541. https://doi.org/10.3109/02713689008999593. [PubMed: 2387165]
40. Crow JM, Atkinson MM, Johnson RG. Micromolar levels of intracellular calcium reduce gap junctional permeability in lens cultures. Invest Ophthalmol Vis Sci. 1994; 35:3332–3341. [PubMed: 8045723]
41. Churchill GC, Lurtz MM, Louis CF. Ca^{2+} regulation of gap junctional coupling in lens epithelial cells. Am J Physiol Cell Physiol. 2001; 281:C972–C981. [PubMed: 11502574]
42. Lurtz MM, Louis CF. Calmodulin and Protein Kinase C regulate gap junctional coupling in lens epithelial cells. Am J Physiol Cell Physiol. 2003; 285:C1475–C1482. https://doi.org/10.1152/ajpcell.00361.2002. [PubMed: 12917107]
43. Peracchia C, Sotkis A, Wang XG, Peracchia LL, Persechini A. Calmodulin directly gates gap junction channels. J Biol Chem. 2000; 275:26220–26224. https://doi.org/10.1074/jbc.M004007200. [PubMed: 10852921]
44. Peracchia C, Wang X, Li L, Peracchia LL. Inhibition of calmodulin expression prevents low-pH-induced gap junction uncoupling in Xenopus oocytes. Pflugers Arch. 1996; 431:379–387. https://doi.org/10.1007/BF02207275. [PubMed: 8584431]
45. Burr GS, Mitchell CK, Keflemariam YJ, Heidelberger R, O'Brien J. Calcium-dependent binding of calmodulin to neuronal gap junction proteins. Biochem Biophys Res Commun. 2005; 335:1191–1198. https://doi.org/10.1016/j.bbrc.2005.08.007. [PubMed: 16112650]
46. Dodd R, Peracchia C, Stolady D, Török K. Calmodulin association with connexin32-derived peptides suggests *trans*-domain interaction in chemical gating of gap junction channels. J Biol Chem. 2008; 283:26911–26920. https://doi.org/10.1074/jbc.M801434200. [PubMed: 18676375]

47. Zhou Y, Yang W, Lurtz MM, Ye Y, Huang Y, Lee H-W, et al. Identification of the calmodulin binding domain of connexin 43. J Biol Chem. 2007; 282:35005–35017. https://doi.org/10.1074/jbc.M707728200. [PubMed: 17901047]
48. Zhou Y, Yang W, Lurtz MM, Chen Y, Jiang J, Huang Y, et al. Calmodulin mediates the Ca^{2+}-dependent regulation of Cx44 gap junctions. Biophys J. 2009; 96:2832–2848. https://doi.org/10.1016/j.bpj.2008.12.3941. [PubMed: 19348766]
49. Chen Y, Zhou Y, Lin X, Wong HC, Xu Q, Jiang J, et al. Molecular interaction and functional regulation of connexin50 gap junctions by calmodulin. Biochem J. 2011; 435:711–722. https://doi.org/10.1042/BJ20101726. [PubMed: 21320072]
50. Suga M, Maeda S, Nakagawa S, Yamashita E, Tsukihara T. A description of the structural determination procedures of a gap junction channel at 3.5 Å resolution. Acta Crystallogr D Biol Crystallogr. 2009; 65:758–766. https://doi.org/10.1107/S0907444909014711. [PubMed: 19622859]
51. Maeda S, Nakagawa S, Suga M, Yamashita E, Oshima A, Fujiyoshi Y, et al. Structure of the connexin 26 gap junction channel at 3.5 Å resolution. Nature. 2009; 458:597–602. https://doi.org/10.1038/nature07869. [PubMed: 19340074]
52. Ghil S, McCoy KL, Hepler JR. Regulator of G protein signaling 2 (RGS2) and RGS4 form distinct G protein-dependent complexes with protease activated-receptor 1 (PAR1) in live cells. PLoS ONE. 2014; 9:e95355. https://doi.org/10.1371/journal.pone.0095355. [PubMed: 24743392]
53. Yap KL, Kim J, Truong K, Sherman M, Yuan T, Ikura M. Calmodulin target database. J Struct Funct Genomics. 2000; 1:8–14. https://doi.org/10.1023/A:1011320027914. [PubMed: 12836676]
54. Mruk K, Farley BM, Ritacco AW, Kobertz WR. Calmodulation meta-analysis: predicting calmodulin binding via canonical motif clustering. J Gen Physiol. 2014; 144:105–114. https://doi.org/10.1085/jgp.201311140. [PubMed: 24935744]
55. Larkin MA, Blackshields G, Brown NP, Chenna R, McGettigan PA, McWilliam H, et al. Clustal W and Clustal X version 2.0. Bioinformatics. 2007; 23:2947–2948. https://doi.org/10.1093/bioinformatics/btm404. [PubMed: 17846036]
56. Putkey JA, Slaughter GR, Means AR. Bacterial expression and characterization of proteins derived from the chicken calmodulincDNA and a calmodulin processed gene. J Biol Chem. 1985; 260:4704–4712. [PubMed: 2985564]
57. Johnson JD, Wittenauer LA. A fluorescent calmodulin that reports the binding of hydrophobic inhibitory ligands. Biochem J. 1983; 211:473–479. https://doi.org/10.1042/bj2110473. [PubMed: 6870843]
58. Whitmore L, Wallace BA. DICHROWEB, an online server for protein secondary structure analyses from circular dichroism spectroscopic data. Nucleic Acids Res. 2004; 32:W668–W673. https://doi.org/10.1093/nar/gkh371. [PubMed: 15215473]
59. VanScyoc WS, Shea MA. Phenylalanine fluorescence studies of calcium binding to N-domain fragments of *Paramecium* calmodulin mutants show increased calcium affinity correlates with increased disorder. Protein Sci. 2001; 10:1758–1768. https://doi.org/10.1110/ps.11601. [PubMed: 11514666]
60. Delaglio F, Grzesiek S, Vuister GW, Zhu G, Pfeifer J, Bax A. NMRPipe: a multidimensional spectral processing system based on UNIX pipes. J Biomol NMR. 1995; 6:277–293. https://doi.org/10.1007/BF00197809. [PubMed: 8520220]
61. Goddard, TD., Kneller, DG. SPARKY 3. University of California; San Francisco:
62. Reddy Chichili VP, Xiao Y, Seetharaman J, Cummins TR, Sivaraman J. Structural basis for the modulation of the neuronal voltage-gated sodium channel NaV1.6 by calmodulin. Sci Rep. 2013; 3:2435. https://doi.org/10.1038/srep02435. [PubMed: 23942337]
63. Feldkamp MD, Yu L, Shea MA. Structural and energetic determinants of apocalmodulin binding to the IQ motif of the $Na_V1.2$ voltage-dependent sodium channel. Structure. 2011; 19:733–747. https://doi.org/10.1016/j.str.2011.02.009. [PubMed: 21439835]
64. Theoharis NT, Sorensen BR, Theisen-Toupal J, Shea MA. The neuronal voltage-dependent sodium channel type II IQ motif lowers the calcium affinity of the C-domain of calmodulin. Biochemistry. 2008; 47:112–123. https://doi.org/10.1021/bi7013129. [PubMed: 18067319]

65. Fielding L. NMR methods for the determination of protein–ligand dissociation constants. Curr Top Med Chem. 2003; 3:39–53. https://doi.org/10.2174/1568026033392705. [PubMed: 12577990]
66. Kincaid RL, Vaughan M, Osborne JC Jr, Tkachuk VA. Ca^{2+}-dependent interaction of 5-dimethylaminonaphthalene-1-sulfonyl-calmodulin with cyclic nucleotide phosphodiesterase, calcineurin, and troponin I. J Biol Chem. 1982; 257:10638–10643. [PubMed: 6286665]
67. Lehrman SR, Tuls JL, Lund M. Peptide α-helicity in aqueous trifluoroethanol: correlations with predicted α-helicity and the secondary structure of the corresponding regions of bovine growth hormone. Biochemistry. 1990; 29:5590–5596. https://doi.org/10.1021/bi00475a025. [PubMed: 2386788]
68. Luo P, Baldwin RL. Mechanism of helix induction by trifluoroethanol: a framework for extrapolating the helix-forming properties of peptides from trifluoroethanol/water mixtures back to water. Biochemistry. 1997; 36:8413–8421. https://doi.org/10.1021/bi9707133. [PubMed: 9204889]
69. Luo P, Baldwin RL. Interaction between water and polar groups of the helix backbone: an important determinant of helix propensities. Proc Natl Acad Sci USA. 1999; 96:4930–4935. https://doi.org/10.1073/pnas.96.9.4930. [PubMed: 10220396]
70. Brokx RD, Scheek RM, Weljie AM, Vogel HJ. Backbone dynamic properties of the central linker region of calcium-calmodulin in 35% trifluoroethanol. J Struct Biol. 2004; 146:272–280. https://doi.org/10.1016/j.jsb.2003.12.007. [PubMed: 15099569]
71. Spyracopoulos L, Li MX, Sia SK, Gagné SM, Chandra M, Solaro RJ, et al. Calcium-induced structural transition in the regulatory domain of human cardiac troponin C. Biochemistry. 1997; 36:12138–12146. https://doi.org/10.1021/bi971223d. [PubMed: 9315850]
72. Peracchia C, Bernardini G, Peracchia LL. Iscalmodulin involved in the regulation of gap junction permeability? Pflugers Arch. 1983; 399:152–154. https://doi.org/10.1007/BF00663912. [PubMed: 6316253]
73. Peracchia C, Bernardini G. Gap junction structure and cell-to-cell coupling regulation: is there a calmodulin involvement? Fed Proc. 1984; 43:2681–2691. [PubMed: 6088292]
74. Peracchia C. Communicating junctions and calmodulin: inhibition of electrical uncoupling in Xenopus embryo by calmidazolium. J Membr Biol. 1984; 81:49–58. https://doi.org/10.1007/BF01868809. [PubMed: 6492129]
75. Peracchia C. Calmodulin-like proteins and communicating junctions. Electrical uncoupling of crayfish septate axons is inhibited by the calmodulin inhibitor W7 and is not affected by cyclic nucleotides. Pflugers Arch. 1987; 408:379–385. https://doi.org/10.1007/BF00581132. [PubMed: 3035483]
76. Hertzberg EL, Gilula NB. Liver gap junctions and lens fiber junctions: comparative analysis and calmodulin interaction. Cold Spring Harb Symp Quant Biol. 1982; 46:639–645. https://doi.org/10.1101/SQB.1982.046.01.060. [PubMed: 6955103]
77. Van Eldik LJ, Hertzberg EL, Berdan RC, Gilula NB. Interaction of calmodulin and other calcium-modulated proteins with mammalian and arthropod junctional membrane proteins. Biochem Biophys Res Commun. 1985; 126:825–832. https://doi.org/10.1016/0006-291X(85)90259-1. [PubMed: 2983692]
78. Zimmer DB, Green CR, Evans WH, Gilula NB. Topological analysis of the major protein in isolated intact rat liver gap junctions and gap junction-derived single membrane structures. J Biol Chem. 1987; 262:7751–7763. [PubMed: 3034905]
79. Alev C, Urschel S, Sonntag S, Zoidl G, Fort AG, Hoher T, et al. The neuronal connexin36 interacts with and is phosphorylated by CaMKII in a way similar to CaMKII interaction with glutamate receptors. Proc Natl Acad Sci USA. 2008; 105:20964–20969. https://doi.org/10.1073/pnas.0805408105. [PubMed: 19095792]
80. Siu RCF, Smirnova E, Brown CA, Zoidl C, Spray DC, Donaldson LW, et al. Structural and functional consequences of connexin 36 (Cx36) interaction with calmodulin. Front Mol Neurosci. 2016; 9:120. https://doi.org/10.3389/fnmol.2016.00120. [PubMed: 27917108]
81. Pfleger KDG, Eidne KA. Illuminating insights into protein-protein interactions using bioluminescence resonance energy transfer (BRET). Nat Methods. 2006; 3:165–174. https://doi.org/10.1038/nmeth841. [PubMed: 16489332]

82. Eidne KA, Kroeger KM, Hanyaloglu AC. Applications of novel resonance energy transfer techniques to study dynamic hormone receptor interactions in living cells. Trends Endocrinol Metab. 2002; 13:415–421. https://doi.org/10.1016/S1043-2760(02)00669-0. [PubMed: 12431837]
83. Pfleger KDG, Eidne KA. Monitoring the formation of dynamic G-protein-coupled receptor–protein complexes in living cells. Biochem J. 2005; 385:625–637. https://doi.org/10.1042/BJ20041361. [PubMed: 15504107]
84. Milligan G, Bouvier M. Methods to monitor the quaternary structure of G protein-coupled receptors. FEBS J. 2005; 272:2914–2925. https://doi.org/10.1111/j.1742-4658.2005.04731.x. [PubMed: 15955052]
85. Germain-Desprez D, Bazinet M, Bouvier M, Aubry M. Oligomerization of transcriptional intermediary factor 1 regulators and interaction with ZNF74 nuclear matrix protein revealed by bioluminescence resonance energy transfer in living cells. J Biol Chem. 2003; 278:22367–22373. https://doi.org/10.1074/jbc.M302234200. [PubMed: 12684500]
86. Olwin BB, Edelman AM, Krebs EG, Storm DR. Quantitation of energy coupling between Ca^{2+}, calmodulin, skeletal muscle myosin light chain kinase, and kinase substrates. J Biol Chem. 1984; 259:10949–10955. [PubMed: 6547956]
87. Olwin BB, Storm DR. Calcium binding to complexes of calmodulin and calmodulin binding proteins. Biochemistry. 1985; 24:8081–8086. https://doi.org/10.1021/bi00348a037. [PubMed: 3004573]
88. Peersen OB, Madsen TS, Falke JJ. Intermolecular tuning of calmodulin by target peptides and proteins: differential effects on Ca^{2+} binding and implications for kinase activation. Protein Sci. 1997; 6:794–807. https://doi.org/10.1002/pro.5560060406. [PubMed: 9098889]
89. Evans TIA, Hell JW, Shea MA. Thermodynamic linkage between calmodulin domains binding calcium and contiguous sites in the C-terminal tail of $Ca_V1.2$. Biophys Chem. 2011; 159:172–187. https://doi.org/10.1016/j.bpc.2011.06.007. [PubMed: 21757287]
90. Xiong LW, Newman RA, Rodney GG, Thomas O, Zhang JZ, Persechini A, et al. Lobe-dependent regulation of ryanodine receptor type 1 by calmodulin. J Biol Chem. 2002; 277:40862–40870. https://doi.org/10.1074/jbc.M206763200. [PubMed: 12185083]
91. Johnson JD, Snyder C, Walsh M, Flynn M. Effects of myosin light chain kinase and peptides on Ca^{2+} exchange with the N- and C-terminal Ca^{2+} binding sites of calmodulin. J Biol Chem. 1996; 271:761–767. https://doi.org/10.1074/jbc.271.2.761. [PubMed: 8557684]
92. Halling DB, Georgiou DK, Black DJ, Yang G, Fallon JL, Quiocho FA, et al. Determinants in Ca_V1 channels that regulate the Ca^{2+} sensitivity of bound calmodulin. J Biol Chem. 2009; 284:20041–20051. https://doi.org/10.1074/jbc.M109.013326. [PubMed: 19473981]
93. Tang W, Halling DB, Black DJ, Pate P, Zhang JZ, Pedersen S, et al. Apocalmodulin and Ca^{2+}calmodulin-binding sites on the $Ca_V1.2$ channel. Biophys J. 2003; 85:1538–1547. https://doi.org/10.1016/S0006-3495(03)74586-X. [PubMed: 12944271]
94. Kim J, Ghosh S, Liu H, Tateyama M, Kass RS, Pitt GS. Calmodulin mediates Ca^{2+} sensitivity of sodium channels. J Biol Chem. 2004; 279:45004–45012. https://doi.org/10.1074/jbc.M407286200. [PubMed: 15316014]
95. Black DJ, Leonard J, Persechini A. Biphasic Ca^{2+}-dependent switching in a calmodulin–IQ domain complex. Biochemistry. 2006; 45:6987–6995. https://doi.org/10.1021/bi052533w. [PubMed: 16734434]
96. Bähler M, Rhoads A. Calmodulin signaling via the IQ motif. FEBS Lett. 2002; 513:107–113. https://doi.org/10.1016/S0014-5793(01)03239-2. [PubMed: 11911888]
97. Shah VN, Wingo TL, Weiss KL, Williams CK, Balser JR, Chazin WJ. Calcium-dependent regulation of the voltage-gated sodium channel hH1: intrinsic and extrinsic sensors use a common molecular switch. Proc Natl Acad Sci USA. 2006; 103:3592–3597. https://doi.org/10.1073/pnas.0507397103. [PubMed: 16505387]
98. Mori M, Konno T, Morii T, Nagayama K, Imoto K. Regulatory interaction of sodium channel IQ-motif with calmodulin C-terminal lobe. Biochem Biophys Res Commun. 2003; 307:290–296. https://doi.org/10.1016/S0006-291X(03)01183-5. [PubMed: 12859953]

99. Houdusse A, Cohen C. Target sequence recognition by the calmodulin superfamily: implications from light chain binding to the regulatory domain of scallop myosin. Proc Natl Acad Sci USA. 1995; 92:10644–10647. https://doi.org/10.1073/pnas.92.23.10644. [PubMed: 7479857]

100. Ikura M, Clore GM, Gronenborn AM, Zhu G, Klee CB, Bax A. Solution structure of a calmodulin-target peptide complex by multidimensional NMR. Science. 1992; 256:632–638. https://doi.org/10.1126/science.1585175. [PubMed: 1585175]

101. Bader P, Weingart R, Egger M. Regulation of Cx45 hemichannels mediated by extracellular and intracellular calcium. Pflugers Arch. 2012; 464:249–259. https://doi.org/10.1007/s00424-012-1133-8. [PubMed: 22733357]

102. Nakase T, Naus CC. Gap junctions and neurological disorders of the central nervous system. Biochim Biophys Acta, Biomembr. 2004; 1662:149–158. https://doi.org/10.1016/j.bbamem.2004.01.009.

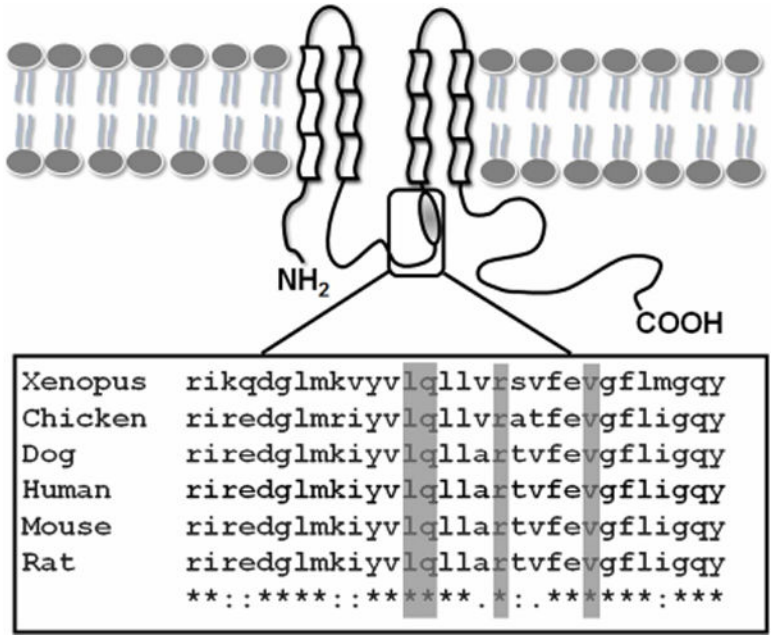

Figure 1. Cx45 membrane topology and the putative CaM-binding site

Cx45 has four transmembrane domains connected by two extracellular loops and one intracellular loop, which is longer than α- and β-class of connexins. The CaM-binding site is located in the second half of the intracellular loop. The predicted CaM-binding motif is conserved in Cx45 from different species.

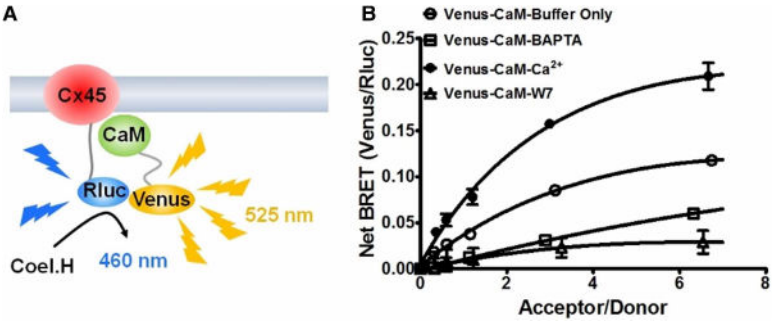

Figure 2. CaM interacts with Cx45 in live cells in a Ca^{2+}-sensitive manner

(**A**) Interaction between CaM and Cx45 was assessed by BRET in live HEK293 cells. HEK293 cells were cotransfected with a fixed amount of Cx45-Rluc and with an increasing DNA concentration of Venus–CaM (expression level was verified by fluorescence intensity measurement). BRET assays were performed 24 h after transfection. Cells were treated with 5 μM coelenterazine, followed by immediate BRET measurement. (**B**) Cells were treated with only BRET buffer, or buffer containing either 50 μM W7, or 5 mM Ca^{2+}/10 μM ionomycin, or 50 μM BAPTA-AM for 30, 10, or 20 min, respectively, before BRET measurement. The net BRET ratios shown above are the mean ± S.E.

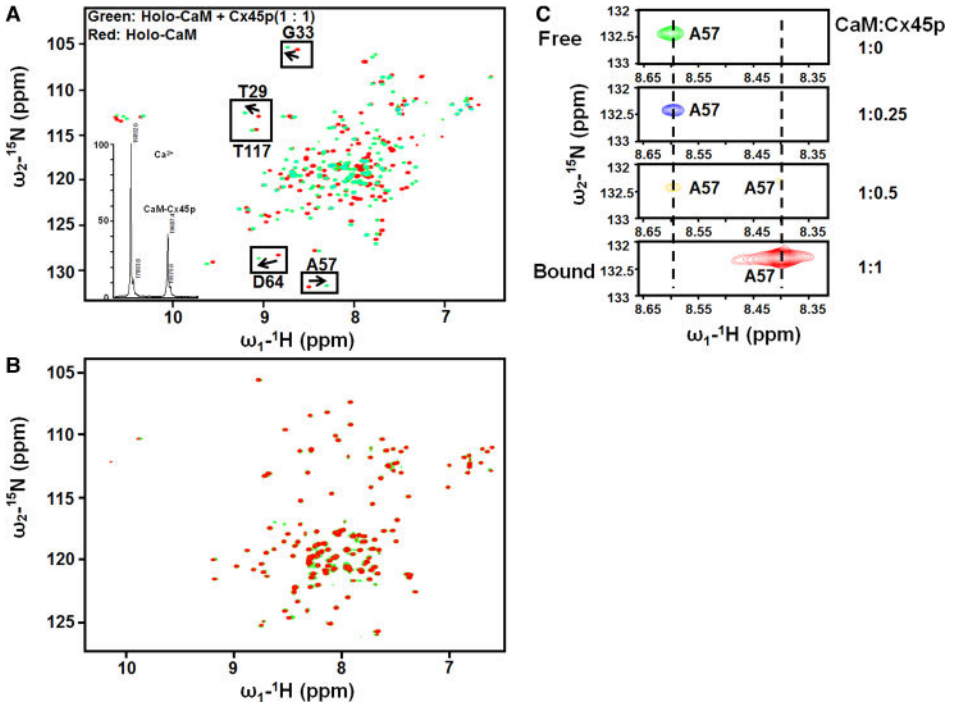

Figure 3. Ca^{2+}-dependent specific interaction between CaM and $Cx45p_{164–186}$ characterized by NMR

(**A**) Overlay of HSQC spectra of holo-CaM (red) with the spectra of holo-CaM–$Cx45p_{164–186}$ complex (green). Inset, the MALDI-MS spectrum of the free form of CaM (left peak) and the CaM–$Cx45p_{164–186}$ complex (right peak) formed in the presence of Ca^{2+}. (**B**) Overlay of HSQC spectrum of apo-CaM with the spectrum of apo-CaM–$Cx45p_{164–186}$ mixture. (**C**) The chemical shift change of A57 during titration of holo-CaM with $Cx45p_{164–186}$. The disappearance of the peak (free form) was accompanied by the appearance of the corresponding peak (bound form) at a shifted position.

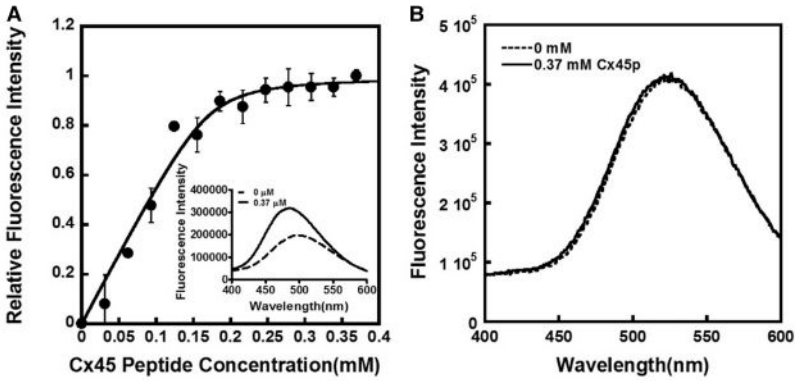

Figure 4. Determination of the CaM–Cx45p$_{164–186}$-binding affinity by steady-state fluorescence studies

(**A**) The titration curve of D-CaM (0.25 μM) with Cx45p$_{164–186}$ in the presence of 5 mM Ca^{2+}. The fluorescence spectra of D-CaM with (solid line) or without Cx45p$_{164–186}$ (dotted line) are seen in the inset. (**B**) The fluorescence spectra of D-CaM (0.25 μM) with 0 or 0.37 μM Cx45p$_{164–186}$ in the presence of 5 mM EGTA. All experiments were repeated in triplicate.

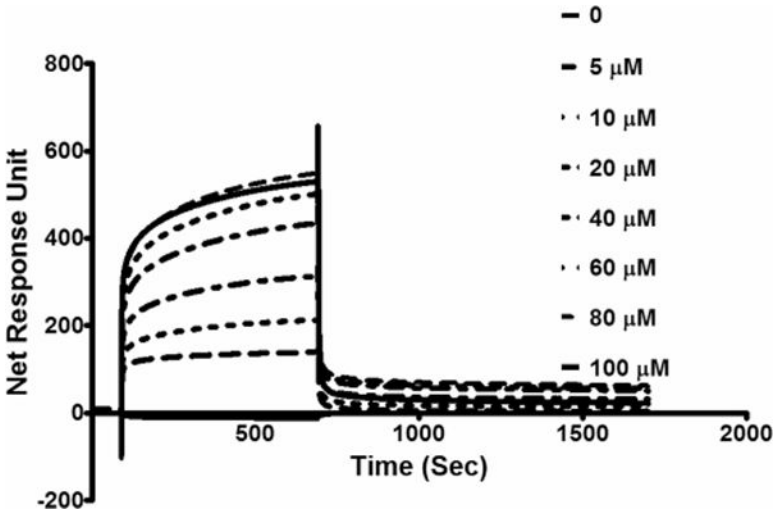

Figure 5. Ca^{2+}-sensitive interaction between CaM and $Cx45p_{164–186}$ is confirmed by SPR analysis

The response unit was recorded with Cx45 peptide immobilized on a CM5 sensor chip under Ca^{2+}-supplemented conditions using a sensitivity-enhanced Biacore T100 SPR system. The concentrations of CaM were 5–100 μM.

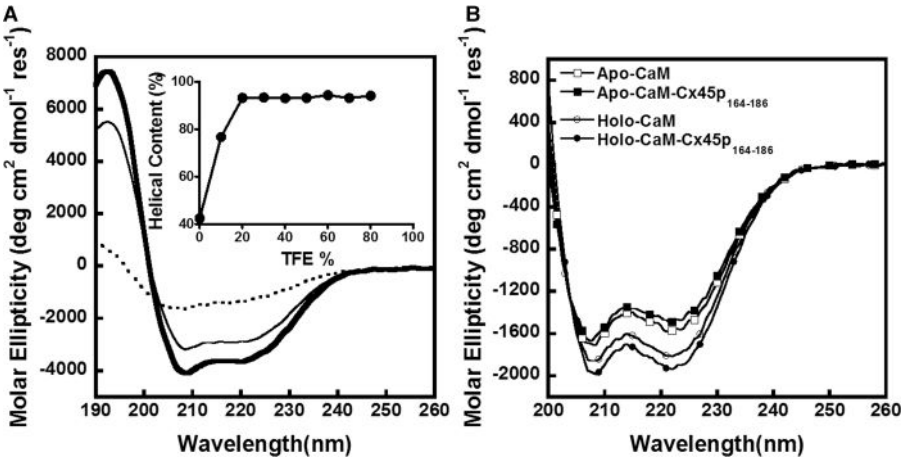

Figure 6. Revealing CaM–peptide interactions with CD spectroscopy

(**A**) Far UV spectra of $Cx45p_{164–186}$ were obtained in the presence of 0% (dotted line), 20% (thin solid line), and 60% (bold solid line) TFE (v/v). Inset: the helical content of $Cx45p_{164–186}$ was plotted against TFE concentration. (**B**) Far UV CD spectra of CaM in the presence of 5 mM EGTA (□) or $CaCl_2$ (○) and a 1 : 1 CaM/$Cx45p_{164–186}$ complex with 5 mM EGTA (■) or $CaCl_2$ (●).

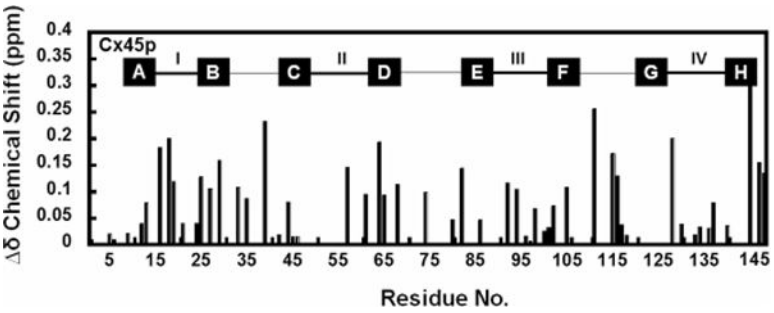

Figure 7. Chemical shift perturbation in CaM induced by Cx45p$_{164–186}$

The weight-average chemical shift changes (Δδ) were calculated and plotted as a function of amino acid residue number. The upper and lower values are chemical shift perturbations in CaM induced by Cx45p$_{164–186}$. The value of Δδ > 0.05 is considered as a significant change.

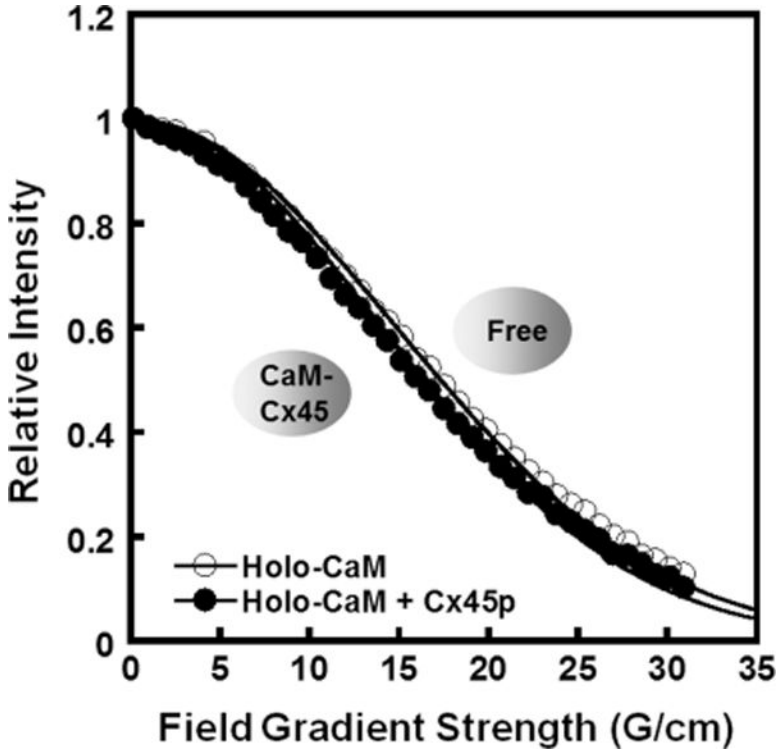

Figure 8. Cx45p$_{164–186}$ binding to CaM without significant hydrodynamic radius change

Hydrodynamics of the holo-CaM–connexin peptide complex were determined by pulsed-field gradient NMR. The holo-CaM (○) NMR signal decay curve did not change upon the addition of Cx45p$_{164–186}$ (●), which indicates that the hydrodynamic radius was not altered.

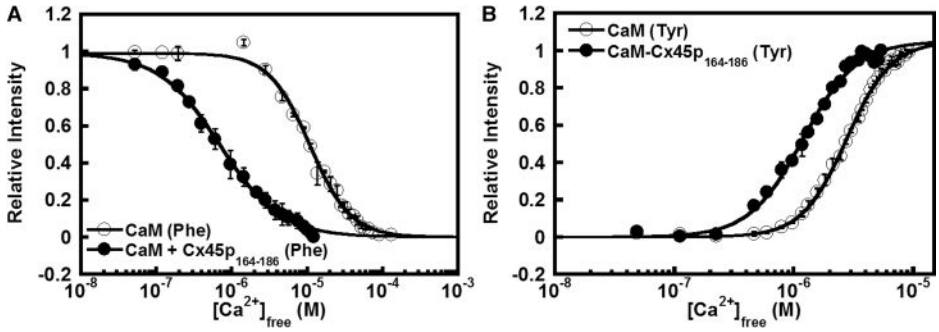

Figure 9. Binding of Cx45p$_{164–186}$ expands the Ca^{2+} sensitivity of both domains of CaM

Equilibrium Ca^{2+} titrations of CaM with (solid cycles) or without (open cycles) Cx45p$_{164–186}$ were evaluated by monitoring fluorescence emission. (**A**) The Phe fluorescence emission changes were utilized to reflect changes in the Ca^{2+}-binding affinity of the N-domain of CaM. (**B**) Changes in CaM C-domain Tyr fluorescence emission upon the addition of Ca^{2+} in the presence or absence of Cx45p$_{164–186}$ were also monitored. Free Ca^{2+} concentration was determined using the Ca^{2+} indicator Oregon Green.

Table 1

Effects of $Cx45p_{164–186}$ binding on the Ca^{2+}-binding properties of CaM

	N-domain		C-domain	
	K_d (μM)	Hill	K_d (μM)	Hill
CaM	11 ± 0.03	1.6 ± 0.07	2.8 ± 0.02	2.3 ± 0.03
CaM–Cx45p	0.7 ± 0.02	1.0 ± 0.03	1.2 ± 0.02	1.9 ± 0.06